Inorganic Chemistry

Article

pubs.acs.org/IC

Synthesis of Luminescent Nanoporous Silica Spheres Functionalized with Folic Acid for Targeting to Cancer Cells

Motohiro Tagaya,*[,†] Toshiyuki Ikoma,[‡] Zhefeng Xu,[§] and Junzo Tanaka[‡]

[†]Department of Materials Science and Technology, Nagaoka University of Technology, 1603-1 Kamitomioka, Nagaoka, Niigata 940-2188, Japan

[‡]Department of Metallurgy and Ceramics Science, Tokyo Institute of Technology, 2-12-1 O-okayama, Meguro-ku, Tokyo 152-8550, Japan

[§]Department of Mechanical Science and Engineering, Hiroshima University, 1-4-1 Kagamiyama, Higashi-Hiroshima, Hiroshima 739-8527, Japan

Supporting Information

ABSTRACT: Luminescent europium(III)-doped nanoporous silica nanospheres (Eu:NPS) were successfully synthesized, and a folate *N*-hydroxysuccinimidyl ester (FA-NHS) molecule as a targeting ligand for cancer cells was immobilized on the nanosphere surfaces through mediation of the 3-aminopropyltriethoxysilane (APTES) adlayer. The ordered nanopores were preserved by the immobilization, and the specific surface area decreased only with the APTES immobilization, suggesting that the FA-NHS was predominantly immobilized on the outer surface of the nanopores. The photoluminescence of the nanospheres functionalized with folic acid (FA) exhibited a characteristic peak due to the interactions (e.g., energy transfer) between FA and Eu^{3+}, and further the orange luminescence could be clearly detected by fluorescence microscopy in air and water. Furthermore, the nanospheres highly dispersed in cell culture medium exhibited nontoxicity in the cellular proliferation stages of the Hela cancer cells and NIH3T3 fibroblasts and specifically bind to the Hela cells. The nanospheres after the binding and uptake also showed intense luminescence from the outer/inner cell surfaces for the culture time of 4 days. Therefore, the luminescent FA-functionalized Eu:NPS nanospheres could be used for specific targeting and imaging abilities for cancer cells.

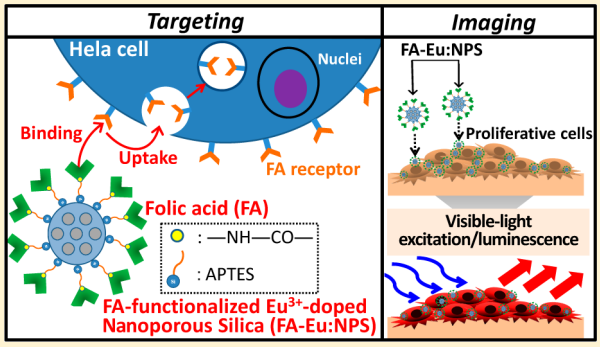

INTRODUCTION

The design of superior imaging and therapeutic nanomaterials against specific cells is very important for use in biomedical science fields. It is known that targeting to the cells through specific ligands or utilizing antibodies depends on the ability of the targeting reagents to selectively bind to the cell surface and to subsequently trigger receptor-mediated endocytosis.[1] The challenges for combining the targeting with imaging into one system are desired using a nanoparticle. However, the coupling of multifunctional groups in a sufficient concentration on the particle surface is difficult because of the limited number of immobilization sites.

Nanoparticles derived from silica sources have been synthesized and structurally designed for developing powerful biocompatible nanoplatforms in the human body.[2,3] After the discovery of mesostructured silicate materials, nanoporous silica (NPS) prepared by the supramolecular templating method possesses attractive features such as a well-defined and controllable pore size, large surface area, and reactive surface.[4−6] The large immobilization capacity of the nanopores for various functional molecules is one of the many attractive features of NPS, accompanied by controlling the nanostructural properties on a nanometer scale such as the pore and particle sizes as well as framework structures.[7−17] Furthermore, the spherical NPS particles lead to the immobilization of anticancer drug molecules on the molecular-sized nanopores, and the surface modification for controlling the silica−drug as well as silica−cell interactions has been attractive for biomedical applications.[18−21]

The preparation of silica-based biohybrids[22,23] and NPS spheres having imaging or therapeutic properties for biofunctions[24−27] has recently been reported. Because of the excellent candidates for such applications, highly luminescent species of quantum dots in the nanopores have emerged for investigating the reactivity with cells as well as the incorporated heterogeneous states;[28−30] however, heteroelements (Cd^{2+}, Hg^{2+}, Se^{2+}, etc.) in the most cases frequently cause some toxic effects. Furthermore, the drug delivery systems that have been synthesized to combine the two-functional imaging and therapeutic moieties on the surfaces have been reported using a fluorescent dye covalently linked to the surface, making them

Received: March 18, 2014
Published: June 12, 2014

   dx.doi.org/10.1021/ic500609g | *Inorg. Chem.* 2014, 53, 6817−6827

Scheme 1. Schemes of the Immobilizations of (i) APTES and (ii) FA-NHS Molecules on the Luminescent Eu:NPS Surfaces and (iii) Targeting and (iv) Imaging of the Proliferated Hela Cells by Visible-Light Excitation and Luminescence

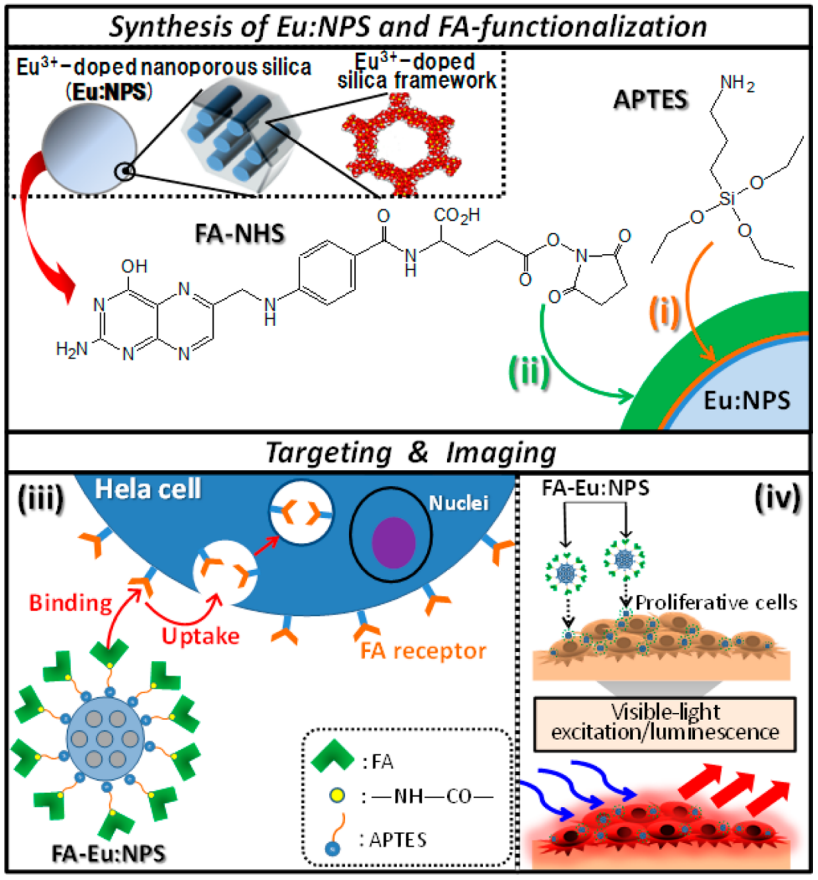

visible by fluorescent microscopy.[31−33] For in vivo applications, some issues of rapid color degradation, excitation by phototoxic light (e.g., UV light), and use of cytotoxic elements should be solved. As a further strategy, if the external surface and silica framework of NPS are functionalized for targeting and imaging, respectively, the internal pore surfaces can be used for the immobilization of therapeutic molecules. In our previous reports, luminescent europium(III) (Eu^{3+})-doped nanoporous silica nanospheres (Eu:NPS) were synthesized,[34,35] and the Eu^{3+}-doped silica frameworks enabled the accommodation of various functional molecules on the internal pore surfaces as well as the immobilization with targeting ligands for cells only on the external surfaces,[36] suggesting the possibility of cellular binding and uptake by their intense luminescence.[37] However, the combinational functions (therapeutic, imaging, and targeting) in one particle using silica spheres with ordered nanoporous structures have not yet been investigated in detail. Therefore, studies on the silica frameworks and external surfaces utilized separately as the luminescent and targeting parts will provide progress in biomedical applications.

In this study, a folic acid (FA) molecule, which has been known as a targeting reagent for cancer cells,[38] was covalently functionalized on the luminescent Eu:NPS nanospheres by the mediation of a 3-aminopropyltriethoxysilane (APTES) adlayer as shown in Scheme 1i,ii, and the photoluminescence as well as the dispersion stability in phosphate-buffered saline were elucidated. Furthermore, the in vitro cytotoxicitiy behavior of the FA-functionalized Eu:NPS nanospheres for Hela cancer cells and NIH3T3 fibroblasts was examined, and targeting and imaging ability for cancer cells was also observed, as shown in Scheme 1iii,iv.

EXPERIMENTAL SECTION

Synthesis of Eu:NPS. Eu^{3+}-doped NPS nanospheres were synthesized according to our previous reports.[34,35] A solution of 1.0 g (2.75 mmol) of cetyltrimethylammonium bromide (CTAB; Wako Co., Ltd.), 225 g of ultrapure water, and 3.5 mL of 2.0 M sodium hydroxide (NaOH; Wako Co., Ltd.) was stirred at 80 °C for 30 min. A 5.515 mL amount (24.7 mmol) of tetraethoxysilane (TEOS; Shinetsu Chemical Co., Ltd.) and then 15 mL of an Eu^{3+} aqueous solution containing 0.226, 0.452, and 0.904 g of $EuCl_3{\cdot}6H_2O$ (Kanto Chemical Co., Ltd.) at initial molar concentrations of Eu^{3+} to Si (Eu/Si) of 2.5, 5.0, and 10 mol % were added, and this mixture was stirred at 80 °C for 2 h. The resulting turbid solution was filtered, and the resulting solids were washed with ultrapure water and ethanol (EtOH; Wako Co., Ltd.) and then vacuumed for 4 h. The CTAB template was completely removed by calcination at 550 °C for 4 h, which had already been reported,[35] and the resulting compounds with Eu/Si concentrations of 2.5, 5.0, and 10 mol % are abbreviated 2.5-Eu:NPS, 5.0-Eu:NPS, and 10.0-Eu:NPS, respectively.

The amount of doped $Eu^{3+}$was determined by an inductively coupled plasma optical emission spectrometer (ICP-OES; Leeman Laboratories, Inc., Prodigy ICP), and the molar concentrations of Eu to Si were 2.78 ± 1.23, 5.40 ± 2.11, and 10.2 ± 3.54 mol % for 2.5-Eu:NPS, 5.0-Eu:NPS, and 10.0-Eu:NPS.[35] As the reference sample, Eu_2O_3 was synthesized by calcination of $EuCl_3{\cdot}6H_2O$, which was identified with ICDD-ICSD 00-034-0072.

Synthesis of Folate *N*-Hydroxysuccinimidyl Ester (FA-NHS). FA-NHS was prepared according to a previous report.[39] A 1.0 g amount of folic acid (FA; Wako Chemical Co., Ltd.), which exhibits an absorbance maxima at 360 nm by a UV−visilble absorption

dx.doi.org/10.1021/ic500609g | Inorg. Chem. 2014, 53, 6817−6827

Table 1. Initial and Equilibrium FA-NHS Concentrations, Functionalized FA Amounts, Surface FA Occupations, d_{100} Values in the XRD Patterns, and ζ-Potential Values of FA-Eu:NPS with Different Immobilization Amounts

sample	initi FA-NHS concn (mM)	functionalized FA amount (μmol (g of APTES**1h**-Eu:NPS)$^{-1}$)	surface FA occupation (%)	d_{100} in the XRD pattern (nm)	ζ potential (mV)
FA**1**-Eu:NPS	0.731	38.9	52.3	3.9	+2.9 ± 0.33
FA**2**-Eu:NPS	1.46	60.8	81.2	3.7	+4.7 ± 0.13
FA**3**-Eu:NPS	2.92	82.0	98	4.2	+7.7 ± 0.07
FA**4**-Eu:NPS	5.85	205	271	4.7	+11.8 ± 0.08
FA**5**-Eu:NPS	11.7	857	1130		+17.6 ± 0.53

spectrometer (Shimazu Co., Ltd., UV-2450), was dissolved in 40 mL of dimethyl sulfoxide (DMSO; Wako Chemical Co., Ltd.) and 0.5 mL of triethylamine (Wako Chemical Co., Ltd.). A 0.52 g amount (2.2 equiv) of *N*-hydroxysuccinimide (NHS; Wako Chemical Co., Ltd.) and 0.50 g (1.1 equiv) of dicyclohexylcarbodiimide (DCC; Wako Chemical Co., Ltd.) were added, and the mixture was then stirred in the dark for 18 h. The resulting turbid solution was filtered in order to remove the precipitated side products (e.g., dicyclohexylurea), and the colature was evaporated under reduced pressure in order to remove triethylamine.

The resulting solution clearly contains FA-NHS, which was confirmed by a ^{1}H NMR analysis, and the solution exhibited an absorbance maximum at 362 nm by the UV−visilble absorption spectrometer. The absorbance maximum at 362 nm of NHS-FA significantly showed a liner relationship with the concentration (see the Supporting Information, Figure S1), leading to a correlation coefficient (R^2) of 0.999 and a molecular extinction coefficient (ε) of 51.9 cm^{-1} M^{-1}.

Immobilizations of APTES and FA-NHS. According to our primary communication report,[36] the APTES immobilization was conducted by stirring the Eu:NPS (250 mg) dispersed into 12 mL of an HCl aqueous solution with the mixed solution of APTES (0.78 mL) and ethanol (5 mL) at 37 °C for 5 h to produce a final pH value of less than 6.5. The suspension was filtered, and the resulting solids were washed with ethanol and subjected to vacuum to finally give the APTES-immobilized Eu:NPS (APTES-Eu:NPS) at the different reaction times of 0, 1, 2, and 5 h, which are abbreviated as APTES**0h**-Eu:NPS, APTES**1h**-Eu:NPS, APTES**2h**-Eu:NPS, and APTES**5h**-Eu:NPS, respectively.

FA-NHS immobilization was conducted by stirring the APTES-Eu:NPS (150 mg) dispersed in 25 mL of a phosphate buffer (PB; pH 7.0, phosphate ion concentration of 50 mM) and 12 mL of a dimethyl sulfoxide (DMSO) solution containing the FA-NHS at 37 °C for 3 h. The suspension was filtered, and the resulting solids were washed by ultrapure water and subjected to vacuum. The immobilization time of FA-NHS was optimized by measuring the immobilization amount of FA-NHS from the initial concentration of 11.7 mM to be 543 μmol (g of APTES-Eu:NPS)$^{-1}$ for 0.5 h, 751 μmol (g of APTES-Eu:NPS)$^{-1}$ for 1 h, 858 μmol (g of APTES-Eu:NPS)$^{-1}$ for 2 h, and 867 μmol (g of APTES-Eu:NPS)$^{-1}$ for 3 h, which were quantitatively determined by the UV−visible absorption spectrometry, indicating the equilibrium time at 2 h. The immobilization amount of FA-NHS was then controlled by five different initial concentrations in solution as shown in Table 1, and the equilibrium concentrations in the solution were 0.257, 1.24, 2.99, 5.44, and 6.79 mM to obtain the objective solids immolibized with FA-NHS amounts of 39, 61, 83, 206, and 858 μmol (g of APTES-Eu:NPS)$^{-1}$, which are abbreviated FA**1**-, FA**2**-, FA**3**-, FA**4**-, and FA**5**-Eu:NPS, respectively.

Characterization of Eu:NPS Immobilized with APTES and FA-NHS. The thermogravimetry (TG) and differential thermal analysis (DTA) changes were recorded in an air atmosphere at a heating rate of 10 K min^{-1} by a TG-DTA instrument (Rigaku Co., Ltd., TG8120). The immobilized APTES amounts were calculated on the basis of the weight loss amount, which approximately corresponds to the aminopropyl chain (M_w = 73.1) in the APTES molecule. The infrared spectra were recorded on a Fourier transform infrared spectrometer (FT-IR; Perkin-Elmer Inc., Spectrum GX) with an accumulation of 128 spectra and resolution of 2.0 cm^{-1}. The X-ray diffraction (XRD) patterns were recorded by a X'Pert Pro MPD instrument (PNAalytical Co., Ltd.) using monochromated Cu Kα radiation. The nanostructures of the spheres were observed on the carbon-coated Cu grid using a transmission electron microscope (TEM; JEOL Co., Ltd., JEM-2010F). The morphologies of the nanospheres were observed using a field emission scanning electron microscope (FE-SEM; Hitachi Co., Ltd., S-4500N). The nitrogen adsorption and desorption isotherms were measured at 77 K by a SA3100 instrument (Bechman Coulter Co., Ltd.). Prior to the measurement, the samples were degassed under vacuum at 393 K for 4 h in APTES-Eu;NPS and at 333 K for 6 h in FA-Eu:NPS. The surface area was evaluated by the BET surface area (S_{BET}), and the pore volume (V) was calculated using the resulting BET surface area and average pore size. The APTES and FA molecular surface occupations were calculated on the basis of molecular areas of 0.38 and 1.65 nm^2, respectively, which were obtained by molecular drawing software (CS Chem 3D Pro). The ζ potential at 25 ± 0.1 °C was performed in phosphate-buffered saline (PBS; pH 7.4, Invitrogen Co., Ltd.) using a laser electrophoresis ζ-potential analyzer (ELS-8000, Otsuka Electronics Co., Ltd.).

The photoluminescence properties were evaluated by photoluminescence spectroscopy and microscopy. The internal quantum efficiency (η_{int}) was measured with a FP-8500 spectrofluorometer (JASCO Co., Ltd.) using an integrating sphere (internal diameter 60 mm). Here, the monitored excitation and luminescence peaks were entered into Figure S4 (Supporting Information) . The incident, scattering, and luminescence light intensity spectra were measured, and their integrated peak intensities were calculated and abbreviated I_0, I_1, and I_2, respectively, as shown in the Supporting Information (Scheme S1). Thus, η_{int} could be calculated by the eq 1. The excitation

$$\eta_{int} = I_2/(I_0 - I_1) \times 100 \quad (1)$$

and luminescence spectra of Eu:NPS, APTES-Eu:NPS, and FA-Eu:NPS were also recorded by the spectrophotometer with the monitored luminescence at 611 nm and excitation wavelength at 464 nm, respectively, at room temperature (atmosphere air, excitation slit/detection slit 2 nm/2 nm, measurement time 0.1 s, step width 1.0 nm, light cut filter on the detection side λ_{cut} <515 nm). The luminescence intensities centered at the top of 550, 590, and 611 nm, which are abbreviated I_{550}, I_{590}, and I_{611}, were calculated by the integrated intensity areas in the ranges 500−570 nm (assigned to a new peak), 580−600 nm (assigned to $^5D_0 \rightarrow {}^7F_1$ of Eu^{3+}), and 600−640 nm (assigned to $^5D_0 \rightarrow {}^7F_1$ of Eu^{3+}) on the basis of the Voigt-function fitting at the peak tops, and the ratios of I_{611} to I_{550} (I_{611}/I_{550}) and of I_{611} to I_{590} (I_{611}/I_{590}) were also calculated. The fluorescence microscope images were obtained using a luminescence microscope (Nikon Co., Ltd., BX-50, excitation wavelength 380−420 nm, exposure time 1500 ms, sensitivity 20).

Cell Culture. Human (Hela) cervical carcinoma cells (RCB0007) and NIH3T3 fibroblasts (RCB1862) as the cell lines, which were provided by the Riken BioResource Center, were separately cultured in a plastic cell culture flask with an area of 75 cm^2 (BD Bioscience) containing 15 mL of fetal bovine serum (FBS; product no. 12603C, lot no. 6D0975, SAFC Bioscience Co., Ltd.) dispersed into Dulbecco's minimum essential medium (DMEM; Invitrogen Co., Ltd.) at a concentration of 10 vol % (10% FBS/DMEM). HeLa cells were used as the cervical cancer model in this study, as they express the folate

dx.doi.org/10.1021/ic500609g | Inorg. Chem. 2014, 53, 6817−6827

receptor-α (FR-α),[48] which can effectively bind with folic acid molecules. On the other hand, NIH3T3 fibroblasts were used as the folate receptor-negative (noncancerous) cell model, and the FR-α concentration is lower in their surfaces. The cells were incubated at 37 °C under a humidified atmosphere of CO_2 (5%) and subcultured every 7 days using 1 mL of 0.05 w/v % trypsin−0.053 M ethylenediaminetetraacetate (trypsin-EDTA; No. 204-16935, Wako Co., Ltd.). After they were washed with 15 mL of PBS and treated with 1 mL of trypsin-EDTA for 10 min at 37 °C, the cells were homogeneously dispersed in 15 mL of PBS, separated by centrifugation (2000 rpm, 2 min), and dispersed in 15 mL of 10% FBS/DMEM. The centrifugation and dispersion were carried out twice, and then the number of cells in the suspension was counted and adjusted at the desired seeding densities for the following experiments.

Cytocompatibility Evaluation of FA-Eu:NPS. The Hela cell and fibroblast suspensions were added and cultured at a seeding area density of 8000 cells/cm^2 on a 96-well poly(styrene) culture plate for evaluating the cell viability (BD Falcon Co., Ltd.) and on a 35 mm tissue culture poly(styrene) dish (TCPS; BD Falcon Co., Ltd.) for counting the number of cells. The cell viability was evaluated using the MTT assay method with 3-(4,5-dimethylthiazol-2-yl)-2,5-diphenyltetrazolium bromide.[40]

At a culture time of 12 h, FA-Eu:NPS dispersed in 10% FBS/DMEM was added to the adhered cell surfaces to adjust the final concentration to 100 μg/mL and then additionally cultured. At a culture time of 24 h, the cell viabilities by Eu:NPS, APTES-Eu:NPS, and FA-Eu:NPS in the 96-well plate were measured and compared. At culture times of 12, 18, 24, 36, 60, and 84 h, the changes in the number of cells by FA**3**-Eu:NPS in the TCPS were also counted. Taking into account the confluence state of 90−100% at the culture time of 60 h as shown in the Supporting Information (Figure S2), the cell viabilities with and without FA**3**-Eu:NPS at culture timed of 24, 36, and 60 h in the 96-well plate were determined. Before the measurements, all of the cell surfaces were washed with PBS twice.

For the viability measurement, 10 μL of the Cell Counting Kit-8 solution (Cayman Chemical Co., Ltd., MTT reagent, Cat. No. 10009591) was added and stored at 37 °C for 3 h under a humidified atmosphere of CO_2 (5%), the solution was removed, and 1 mL of crystal dissolving solution (Cayman Chemical Co., Ltd., Cat. No. 10009593) was added, and the mixture was shaken for 1 min. The absorbance at 570 nm of the resulting solution was then measured by a microplate spectrophotometer (Power Scan HT, DS Pharma Biomedical Co., Ltd.) and the absorbance of 1 mL of 10% FBS/DMEM without addition of FA**3**-Eu:NPS was subtracted as the blank value. The average value of 10 samples was used, and the maximum absorbance in all of the samples was set at 100%.

Cancer Cell Detection Ability Evaluation. The Hela cell and fibroblast suspensions were added and cultured at a seeding area density of 8000 cells/cm^2 on the TCPS for observing the cellular reactions and on the 96-well plate for measuring the luminescence intensity. At s culture time of 12 h, FA**3**-Eu:NPS dispersed in 10% FBS/DMEM was added to the adhered cell surfaces to adjust to the final concentration of 100 μg/mL and then cultured.

For observation of the cellular reactions, the cells on the TCPS dish were cultured for 2 days. At culture times of 14, 18, 20, 24, and 36 h, which correspond to the subsequent culture times of 2, 4, 8, 12, and 24 h after adding FA**3**-Eu:NPS, the cultured cells were fixed with 3.7 vol % formaldehyde in PBS for 10 min. Before and after the fixation, the cells were washed twice with 1 mL of PBS and twice with 1 mL of ultrapure water. The cellular nuclei were then stained with 1 mL of a 4′,6-diamino-2-phenylindole (DAPI; Invitrogen Co., Ltd.) solution which was diluted 15 times into PBS, incubated in the dark for 20 min, and washed twice with 1 mL of PBS and once with 1 mL of ultrapure water. Immediately, the cells in the PBS were observed by the transmitted bright-field and fluorescent images. The fluorescence microscope images were obtained using a luminescence microscope (Nikon Co., Ltd., BX-50; excitation wavelength 380−420 nm, exposure time 1500 ms, sensitivity 20). At a culture time of 24 h, the cells were clearly adhered on the TCPS, as shown in the transmitted bright-field images of Figure S3a,c (Supporting Information) and significantly exhibited no luminescenc,e as shown in the fluorescence images of Figure S3b,d.

For measurement of the luminescence intensity, the cells on the 96-well plate were cultured for 1, 2, 3, 4, and 5 days. After the culture was carried out, the living cells on the 96-well plate were washed twice with 100 μL of PBS and twice with 100 μL of ultrapure water, and immediately the luminescence intensity from the cells was measured by the microplate spectrophotometer at an excitation wavelength of 485 ± 40 nm, a detected wavelength of 590 ± 35 nm, and a sensitivity value of 120.

RESULTS AND DISCUSSION

Synthesized Eu:NPS. The Eu:NPS nanospheres having nanometer particle sizes (ca. 300−1000 nm) were successfully synthesized, and the highly ordered nanopores were preserved by the Eu^{3+} doping, as described in our previous reports.[34,35] As shown in the Supporting Information (Figure S4), the internal quantum efficiencies for 2.5-Eu:NPS, 5.0-Eu:NPS, and 10.0-Eu:NPS were 6.51, 8.67, and 3.91%, respectively, whereas that of Eu_2O_3 was 2.16%, indicating the highest efficiency of 5.0-Eu:NPS. The Eu^{3+} states in the silica framework structures have also been investigated in our previous reports.[35] The O−Si−O and Si−OH groups in the framework structures varied with the interactions of the Eu^{3+} ions with the inner O atoms. The Eu^{3+} ions were located inside the structure to electrostatically interact with the environmental O atoms, which would prevent aggregation among the Eu^{3+} ions, and show the highly efficient luminescence, especially of 5.0-Eu:NPS. This finding on the Eu^{3+} ion dispersion is a merit in the use of nanoporous silicas with ordered structures containing lanthanide ions. Therefore, the luminescent Eu:NPS nanospheres were successfully synthesized by changing the interaction between the Eu^{3+} ions and silica framework structures, and 5.0-Eu:NPS exhibits the highest efficiency. Accordingly, 5.0-Eu:NPS, which is simply abbreviated as Eu:NPS, is used in the following experiments.

APTES Immobilization on Eu:NPS. Figure S5 in the Supporting Information shows the FT-IR spectra of Eu:NPS immobilized with APTES at different reaction times. In APTES**0h**-Eu:NPS, bands at 1070 and 1225 cm^{-1} attributed to the asymmetric and symmetric Si−O−Si stretching were clearly observed. The bands at around 795 and 960 cm^{-1} are assigned to Si−OH stretching, and the band centered at around 3450 cm^{-1} is attributed to O−H stretching. These characteristic bands almost correspond to those in our previous reports.[34,35] With increasing immobilization time, the bands at around 960 and 3450 cm^{-1} decreased, indicating a condensation reaction with the hydroxyl groups of APTES. Simultaneously, the bands at 1560 cm^{-1} due to the N−H in-plane bending deformation, at 2880 cm^{-1} due to the $-CH_2-$ symmetric stretching, and at 2930 cm^{-1} due to the $-CH_2-$ asymmetric stretching newly appeared in the immobilization time, indicating successful APTES immobilization.[36]

Figure 1a shows the N_2 adsorption and desorption isotherms of APTES-Eu:NPS at different reaction times, and the insets give TEM images of APTES**0h**-Eu:NPS. The TEM images clearly exhibit highly ordered nanopore arrangements. The cylindrical pores were homogeneously formed on the nanosphere surfaces, the pore diameter was estimated to be 2.4−2.7 nm, the pore wall thickness was 0.6−1.0 nm, and no guest substances in the pores could be observed. A hysteresis between the adsorption and desorption at a relative pressure of around 0.5 was clearly observed, indicating the formation of mesopores and structural preservation with the immobilization time for an immobilization time of 2 h. The APTES

dx.doi.org/10.1021/ic500609g | Inorg. Chem. 2014, 53, 6817−6827

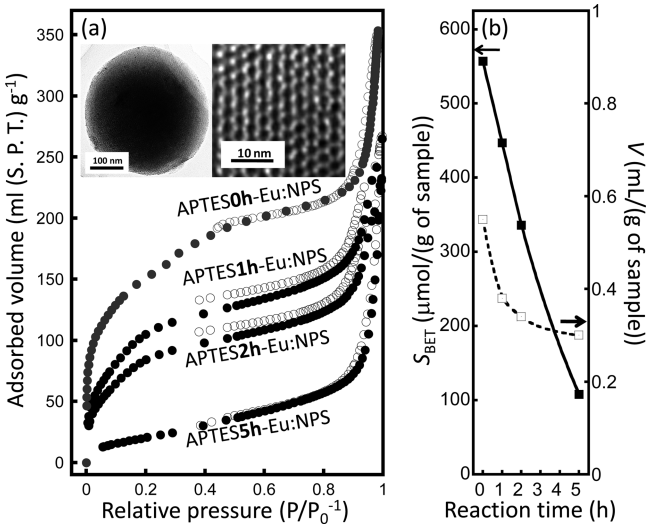

Figure 1. (a) N_2 adsorption (closed circles) and desorption (open circles) isotherms of APTES-Eu:NPS at different reaction times. The insets give TEM images of APTES**0h**-Eu:NPS nanosphere surfaces. (b) S_{BET} (closed squares) and V (open squares) changes versus the reaction time.

immobilization changed the specific surface area from 557 m^2 g^{-1} for Eu:NPS to 447 m^2 g^{-1} at 1 h, to 336 m^2 g^{-1} at 2 h, and to 108 m^2 g^{-1} at 5 h, indicating a linear decrease with reaction time as shown in Figure 1b.

Figure S6 in the Supporting Information shows the TG and DTA curves of Eu:NPS immobilized with APTES at different reaction times. In all of the samples, a small weight loss above 550 °C due to condensation among the remaining silanol groups was slightly observed.[41] In APTES-Eu:NPS, a large weight loss from 160 to 500 °C with an exothermic peak due to the decomposition of the aminoalkyl chain in APTES was clearly observed, with complete removal at around 550 °C. The weight loss in Eu:NPS was much lower than that in APTES-Eu:NPS. Furthermore, the immobilized amount of APTES experimentally estimated by the TG-DTA measurements was 0.43 μmol g^{-1} for 1 h, 0.51 μmol g^{-1} for 2 h, and 0.97 μmol g^{-1} for 5 h. The surface occupation rate is greater than 100% on the Eu:NPS surfaces (Table 2) on the basis of the APTES molecular area of 0.38 nm^2, indicating successful immobilization on the inner and outer mesopore surfaces as well as multilayer formation by condensation among the silanol groups of APTES.

Figure 2a shows the XRD patterns of APTES-Eu:NPS at different reaction times. The peaks in APTES**0h**-Eu:NPS are indexed as the (100), (110), (200), and (220) reflections of a hexagonal structure, suggesting ordered pore arrangements. APTES**1h**-Eu:NPS and APTES**2h**-Eu:NPS preserved the ordered structures on the basis of the d_{100} values (Table 2), although the diffractions with the APTES immobilization deteriorated the arrangements to form worm-like nanopores. Therefore, APTES immobilization on Eu:NPS was successfully achieved, and the pores were preserved by the immobilization. Moreover, FE-SEM images of APTES-Eu:NPS at different reaction times, which indicated the homogeneous and spherical nanospheres, are shown in Figure 2b–i. The images exhibit an average diameter of 380 ± 62 nm for Eu:NPS,[35] and the APTES immobilization significantly induced the morphological changes as well as the particle size increase, implying the formation of siloxane gel networks due to APTES condensation reactions at the multilayers.

The ζ-potential value changes with the APTES immobilization were measured as shown in Table 2. The immobilization can easily be followed by the ζ potential, which is mainly sensitive to the outer surface of the nanospheres. Thus, there is a difference due to the presence of APTES that has positively charged $-NH_2$ groups; the amino group should increase the ζ potential. Whereas the ζ potential of Eu:NPS is negative, the value increased with immobilization time, indicating that the amino group is conjugated to the Eu:NPS surfaces and is stably functionalized in PBS. Taking into account all of the above results, APTES**1h**-Eu:NPS is the most appropriate species; it was then used in the following experiments.

FA Functionalization on APTES-Eu:NPS. The initial FA concentrations, FA functionalization amounts, and surface FA occupations of FA-Eu:NPS with the different functionalization amounts are shown in Table 1. With FA functionalization on APTES-Eu:NPS, bands at 1513, 1608, and 1691 cm^{-1} newly appeared due to the C=C, N–H, and C=O stretching of FA, respectively. As discussed in our previous report,[36] FA functionalization with covalent bonding on APTES-Eu:NPS was achieved. The functionalized amount was controlled by the initial concentration and was photospectroscopically determined to be 38.9 μmol g^{-1} in FA**1**-Eu:NPS, 60.8 μmol g^{-1} in FA**2**-Eu:NPS, 83.0 μmol g^{-1} in FA**3**-Eu:NPS, 205 μmol g^{-1} in FA**4**-Eu:NPS, and 857 μmol g^{-1} in FA**5**-Eu:NPS. In FA**4**-Eu:NPS and FA**5**-Eu:NPS, the surface occupation rate is greater than 100% of the APTES-Eu:NPS surfaces (Table 1) on the basis of the area of the monomeric FA molecule of 2.6 nm^2, indicating the aggregation states among the FA molecular interactions. Thus, the samples with the appropriate functionalization amounts without the aggregation are FA**1**Eu:NPS, FA**2**-Eu:NPS, and FA**3**-Eu:NPS in this study. Taking into account the APTES and FA molecular sizes, the pore size of Eu:NPS (ca. 2.4–2.7 nm) is large enough to accommodate APTES into the nanopores; the internal nanopore size only immobilized with APTES in the monolayer state is approximately 0.5 nm, whereas FA cannot be incorporated into the nanopores, indicating FA functionalization only on the external surfaces as shown in the Supporting Information (Scheme S2).

Table 2. Immobilized APTES Amounts, Surface APTES Occupations, d_{100} Values in the XRD Patterns, and ζ-Potential Values of APTES-Eu:NPS with Different Immobilization Times

sample	immobilized APTES amount (mmol (g of Eu:NPS)$^{-1}$)	surface APTES occupation (%)	d_{100} value in the XRD pattern (nm)	ζ potential (mV)
APTES**0h**-Eu:NPS			3.6	−6.2 ± 0.33
APTES**1h**-Eu:NPS	0.43	193	3.9	−2.3 ± 0.04
APTES**2h**-Eu:NPS	0.51	227	3.9	−1.8 ± 0.08
APTES**5h**-Eu:NPS	0.97	398	–	−1.2 ± 0.05

dx.doi.org/10.1021/ic500609g | Inorg. Chem. 2014, 53, 6817–6827

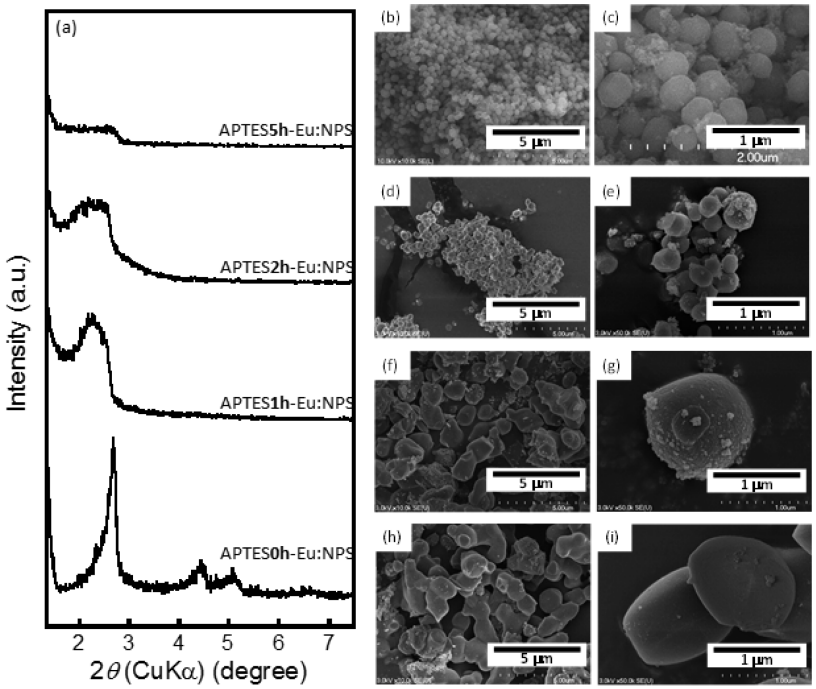

Figure 2. (a) XRD patterns and (b–i) FE-SEM images (magnification (b, d, f, h) ×10000 and (c, e, g, i) ×50000) of APTES-Eu:NPS at different reaction times ((b, c) 0 h, (d, e) 1 h, (f, g) 2 h, and (h, i) 5 h), leading to the optimized reaction time of 1 h as described in the text.

Figure 3 shows the N_2 adsorption and desorption isotherms of FA-Eu:NPS at different functionalization amounts and S_{BET}

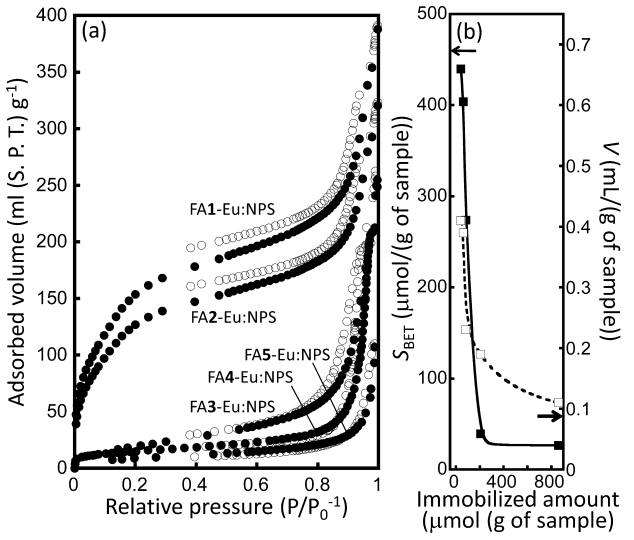

Figure 3. (a) N_2 adsorption (closed circles) and desorption (open circles) isotherms of FA-Eu:NPS at different FA functionalization amounts and (b) S_{BET} (closed squares) and V (open squares) changes versus the reaction time.

and V changes. The hysteresis loop at the higher relative pressure of about 0.9 can be attributed to the interparticle porosity. On the other hand, the hysteresis between the adsorption and desorption at a relative pressure of about 0.5–0.8 was clearly observed in FA**1**-Eu:NPS, FA**2**-Eu:NPS, and FA**3**-Eu:NPS, indicating the formation of mesopores and structural preservation. Figure 3b shows the structural changes, and the specific surface area of the FA functionalization is 440 $m^2\ g^{-1}$ for FA**1**-Eu:NPS, 404 $m^2\ g^{-1}$ for FA**2**-Eu:NPS, and 274 $m^2\ g^{-1}$ for FA**3**-Eu:NPS to 39.6 $m^2\ g^{-1}$ and decreased at the initial concentrations, suggesting that the FA-NHS dispersed inside the APTES-functionalized nanopore surfaces would enhance the roughness and ordering of the pores. Therefore, FA functionalization on the Eu:NPS was successfully achieved, and the ordered nanopores were preserved by the functionalization at the initial concentrations.

Figure 4 shows the XRD patterns of FA-Eu:NPS with different functionalization amounts and the representative FE-SEM image of FA**3**-Eu:NPS. The d_{100} values in the XRD patterns with different functionalization amounts are shown in Table 1. FA was effectively functionalized on APTES-Eu:NPS to give yellow products, as shown in the insets of Figure 4. The FA-Eu:NPS nanospheres, with the exception of FA**5**-Eu:NPS, preserved the ordered structures on the basis of the d_{100} values (Table 1); however, the diffractions with FA functionalization at the higher concentration significantly deteriorated the arrangements. Furthermore, the nanosphere in Figure 4b, which is representative of FA**3**-Eu:NPS, exhibits a particulate shape with a size of ca. 300 nm. To validate the applicability of our nanospheres for targeting to cancer cells by the direct spray/injection of the suspension, we can suggest the non-cytotoxic FA-Eu:NPS with a mean diameter of about 300–400 nm, which was purposefully chosen since smaller nanoparticles show an enhanced nonspecific cellular uptake. In fact, Lin et al. have also shown that surface-functionalized silica particles with a size of 100 nm are effectively internalized by HeLa cells regardless of the surface composition of the particles.[46] Moreover, for amorphous silica, the toxicity tends to be inversely related to the particle size, and a particle size below 100 nm has actually been found to induce cytotoxicity.[47]

Table 1 shows the ζ-potential values of the FA-Eu:NPS with different functionalization amounts. The ζ potential of APTES-Eu:NPS increased with FA functionalization to indicate positive charges, reflecting the pronounced increase in the surface FA density.[26] Therefore, the surface immobilization of FA-NHS on

dx.doi.org/10.1021/ic500609g | Inorg. Chem. 2014, 53, 6817–6827

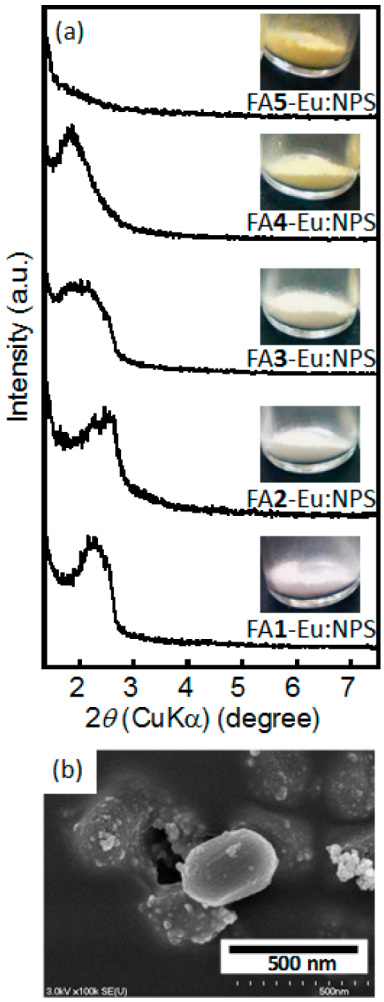

Figure 4. (a) XRD patterns of FA-Eu:NPS with the different FA functionalization amounts (insets give photographs of FA-Eu:NPS) and (b) a representative FE-SEM image of FA**3**-Eu:NPS (magnification ×10000).

the APTES-Eu:NPS surfaces were successful. The ζ-potential value at the physiological pH of 7.4 was +2.9 ± 0.33 mV for FA**1**-Eu:NPS, +4.7 ± 0.13 mV for FA**2**-Eu:NPS, and +7.7 ± 0.07 mV for FA**3**-Eu:NPS, which would make the nanospheres fully dispersible in water.[36]

Photoluminescence Properties. Figure 5 shows the excitation and photoluminescence spectra of Eu:NPS, APTES-Eu:NPS, and FA**3**-Eu:NPS. The inset gives a fluorescence microscope image of FA**3**-Eu:NPS. The excitation and luminescence spectra of FA and NHS-FA in the solid state under the same conditions as in Figure 5 are shown in the Supporting Information (Figure S7), indicating no luminescence from the FA and FA-NHS molecules alone. If we take into account all the previous results, FA**1**-Eu:NPS, FA**2**-Eu:NPS, and FA**3**-Eu:NPS are appropriate, and then FA**3**-Eu:NPS was used as a representative in the following experiments. With the immobilizations, the charge-transfer band at 240 nm in the excitation spectra (detected emission at 611 nm) increased, which was located at a shorter wavelength in comparison to that of the other oxides,[42] suggesting the interaction of the O atoms of APTES with the near-surface Eu^{3+} ions. As described in our previous report,[36] the luminescence spectral shapes clearly depended on the FA amount, and the narrow peaks are attributed to the f−f transitions due to the 4f orbitals of Eu^{3+}.[43] The peaks of APTES-Eu:NPS correspond to the transitions from the metastable orbital singlet state of $^5D_0$ to the spin−orbital states of ^7F_J (J = 0−3),[44] which indicates transitions from $^5D_0$ to $^7F_0$ at 577 nm, to $^7F_1$ at 590 nm, to $^7F_2$ at 611 nm, and to $^7F_3$ at 700 nm, and the luminescence intensity is 0.2 times weaker than that of Eu:NPS. With an increase in FA amount, the broad luminescence peak at around 550 nm was enhanced. If we take into account no luminescence of the neat FA and NHS-FA, the spectral change can be attributed to the excitation of the conjugation band between the FA molecules and near-surface Eu^{3+} ions (e.g., electron transfer from the T_1 level energy of FA to 4f orbitals of Eu^{3+}), implying an effective charge transfer transition. The luminescence of the Eu^{3+} doped in the silica framework was predominantly attributed to $^5D_0 \rightarrow {}^7F_1$ and $^5D_0 \rightarrow {}^7F_2$, and the $^5D_0 \rightarrow {}^7F_2$ intensity depended on the site environment of Eu^{3+}.[34,35,45] The ratio of $^5D_0 \rightarrow {}^7F_2$ to $^5D_0 \rightarrow {}^7F_1$ luminescence intensities (I_{611}/I_{590}) was almost constant with the immobilizations. The integral luminescence intensity and the I_{550}/I_{611} ratio had clearly changed, and these values were at a maximum at FA amounts of 60.3 and 83.0 μmol (g of APTES-Eu:NPS)$^{-1}$, respectively, suggesting the optimum FA molecular states on the surfaces as described in our previous report.[36] Furthermore, the immobilized spheres were easily imaged by the luminescence microscope, as shown in the inset of Figure 5b, indicating the blue shift in comparidon to Eu:NPS alone.[34,35] The decrease with the much higher increase in the FA amount can be attributed to radiationless deactivation by the interactions (e.g., $\pi-\pi$ stacking) among the FA molecules. Therefore, the FA functionalization effectively induced the characteristic luminescence by the band due to the chelate complex (i.e., FA−Eu^{3+}), suggesting the importance of controlling the Eu^{3+} concentration as well as the interactions among the FA molecules. In the following experiment, FA**3**-Eu:NPS was used because the integral luminescence intensity and the I_{550}/I_{611} were at a maximum.

According to our previous report on the UV−visible absorption spectral changes of the FA-Eu:NPS nanospheres dispersed into PBS at a concentration of 500 μg/mL,[36] FA**3**-Eu:NPS was easily dispersed into the PBS (see the Supporting Information, Figure S8a), and the absorbance at 500 nm gradually decreased with the static time, but no spectral shape change occurred. The absorbance for Eu:NPS and APTES**1h**-Eu:NPS decreased by 60−70% for 7 h, whereas that for FA**3**-Eu:NPS decreased by 40%, indicating the significant dispersion stability by the FA functionalization. These results can be attributed to the different surface charges at a certain pH (i.e., positive charge of the FA-functionalized surfaces).[26] Furthermore, FA**3**-Eu:NPS in PBS also exhibited a strong luminescence, as shown in the Supporting Information (Figure S8b), indicating effective utilization in the physiological saline solution as a bioimaging nanomaterial.

Cytocompatibility. Since it is known that toxicity can be observed within 24 h, the cell viabilities of Eu:NPS, APTES-Eu:NPS, and FA-Eu:NPS with the different FA functionalization amounts at 12 h after their addition (culture time 24 h) were investigated, as shown in Figure 6. The adhered cells with the different nanospheres proliferated and maintained their normal morphologies. The cell viability with APTES-Eu:NPS is the lowest due to the influence of the activated amino groups. With increasing FA-functionalization amounts, the cell viability significantly increased, indicating noncytotoxicity of the FA-

dx.doi.org/10.1021/ic500609g | Inorg. Chem. 2014, 53, 6817−6827

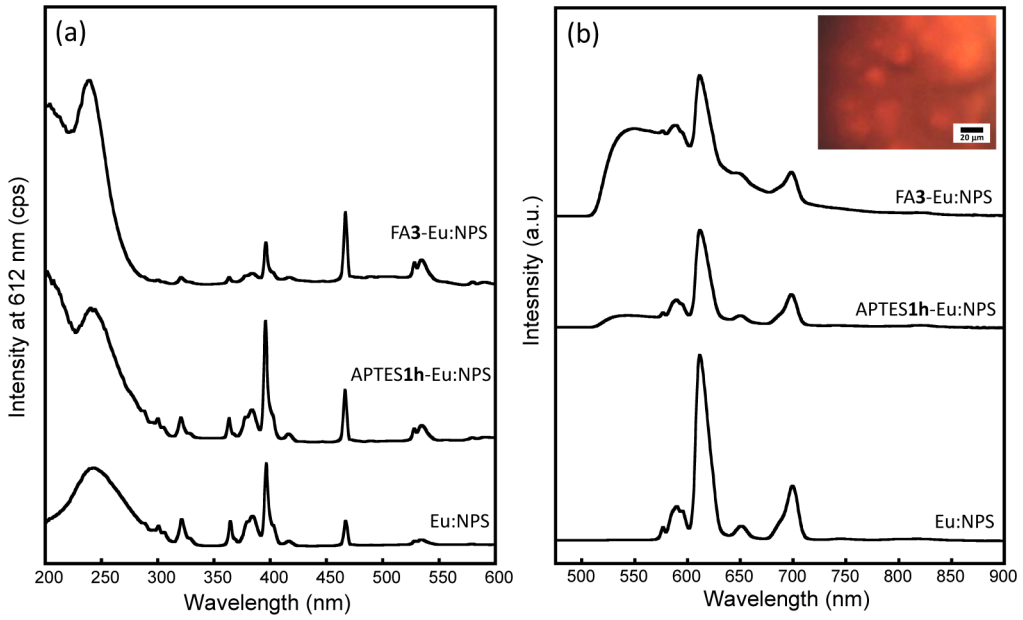

Figure 5. (a) Excitation and (b) photoluminescence spectra of Eu:NPS, APTES**1h**-Eu:NPS, and FA**3**-Eu:NPS. The inset gives a fluorescence microscope image of FA**3**-Eu:NPS.

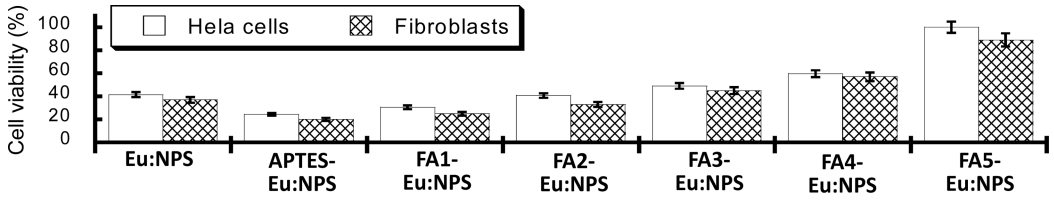

Figure 6. Cell viabilities of Eu:NPS, APTES-Eu:NPS, and FA-Eu:NPS with different FA functionalization amounts at a culture time of 24 h.

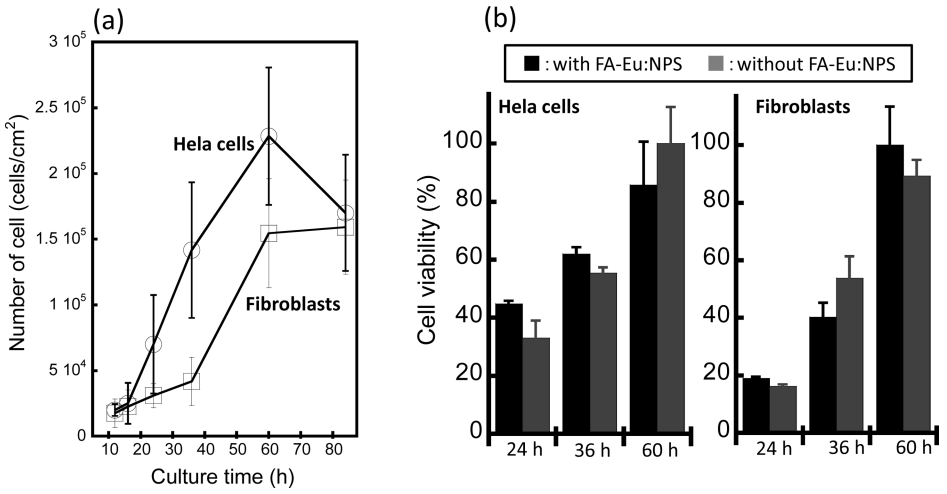

Figure 7. (a) Changes in the number of Hela cells (open circles) and fibroblasts (open squares) with FA**3**-Eu:NPS with the culture time. (b) Cell viability changes with and without FA**3**-Eu:NPS at the different culture times of 24, 36, and 60 h.

functionalized Eu:NPS nanospheres. This indicated that the amino group was deactivated with the FA-NHS functionalization and the FA molecules were functionalized on the surfaces to exhibit a good cytocompatibility; FA**5**-Eu:NPS showed the highest cell viability.

Taking into account these results, FA**3**-Eu:NPS was used as a representative in the following experiment. To investigate the cytocompatibility of FA**3**-Eu:NPS in detail, the changes in the number of Hela cells and fibroblasts with FA**3**-Eu:NPS with the culture time and the cell viability changes with and without FA**3**-Eu:NPS at different culture times were investigated, as shown in Figure 7. For the measurement of the changes in the number of cells, the proliferation behaviors with the addition of FA**3**-Eu:NPS reached the confluent states at a culture time of around 60 h (Figure 7a). In particular, the Hela cells drastically proliferated starting from the time of 16 h and the number of the Hela cells at the confluent state was 1.5 times higher than that of fibroblasts. This behavior is the same as that without the

dx.doi.org/10.1021/ic500609g | Inorg. Chem. 2014, 53, 6817−6827

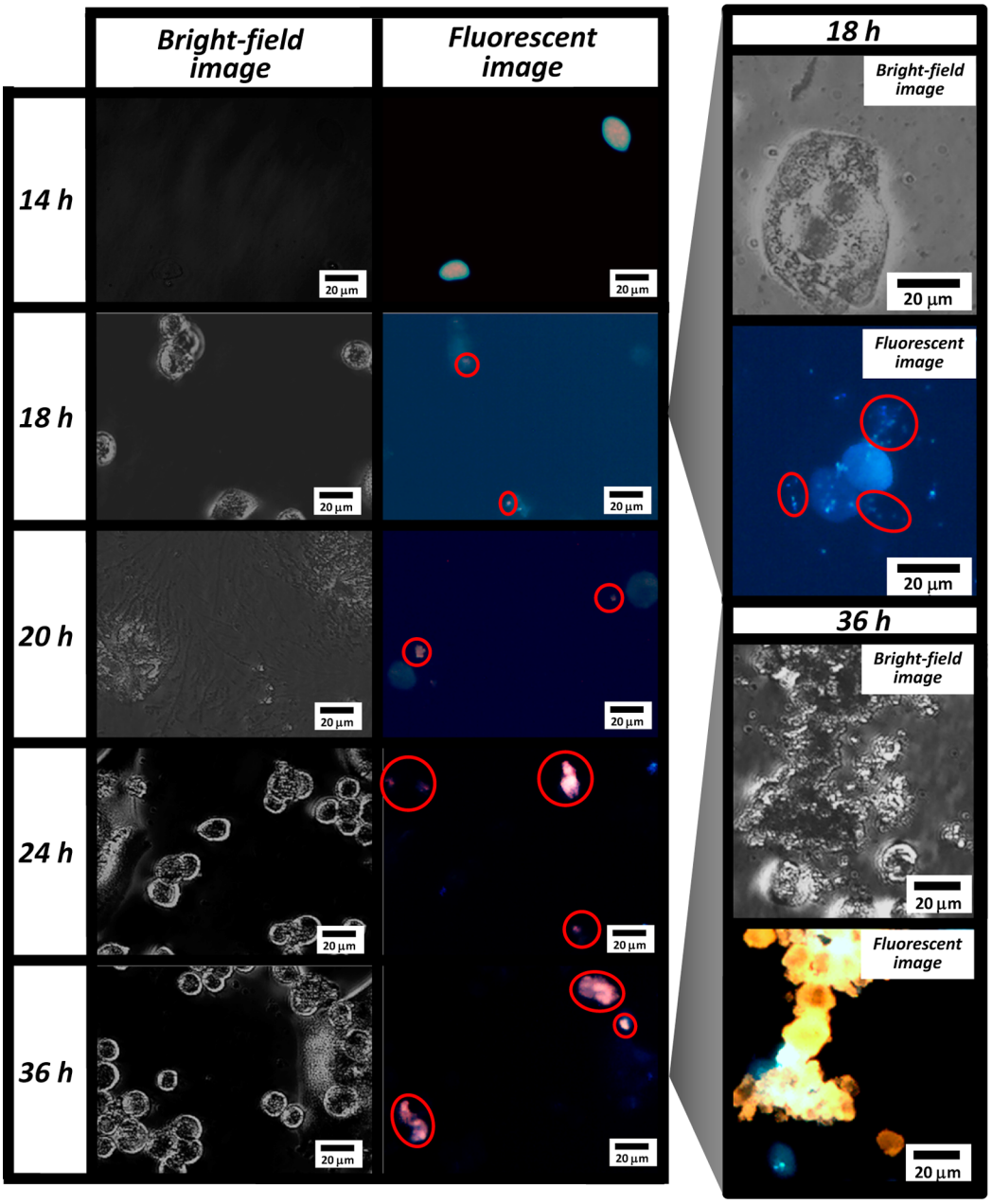

Figure 8. Transmitted bright-field and fluorescent images of the Hela cells reacted with FA3-Eu:NPS at different culture times and representative magnified images of the Hela cells exhibiting the effective reactions (binding and uptake) at times of 18 and 36 h.

nanospheres, indicating the reflection of the native different proliferation rate among the cell lines. Subsequently, the MTT cell viability measurements were conducted for 60 h. The proliferation behaviors with the added FA3-Eu:NPS were almost the same as those without added FA3-Eu:NPS, indicating the significant noncytotoxicity of the FA-functionalized Eu:NPS. Therefore, these results indicated that the FA molecules successfully functionalized on the Eu:NPS exhibit the normal proliferation behaviors on the basis of the high cytocompatibility.

Detection Ability for Cancer Cells. Figure 8 shows the transmitted bright-field and fluorescent images of the Hela cells that reacted with FA3-Eu:NPS at different culture times and the representative magnified images of the Hela cells reacting with FA3-Eu:NPS at times of 18 and 36 h. The luminescence was easily observed by fluorescence microscopy. The fluorescence microscope images show blue luminescence from the cellular nuclei due to the DAPI staining. Significant binding and uptake by the Hela cells were clearly observed. On the other hand, the transmitted bright-field and fluorescence images of the fibroblasts that reacted with FA3-Eu:NPS at different culture times are shown in the Supporting Information (Figure S9), indicating very weak luminescence from the fibroblasts, although there is a difference in the nuclear staining colors between Figure 8 and Figure S9 because the proliferating states (e.g., the number of cells (Figure 7a)) between the Hela cancer cells and fibroblasts are clearly different at the same culture time, which reflects the staining states with the same reagent amount. The fluorescence images of the Hela cells indicate the presence of luminescent nanospheres located around the nucleus at a time of 4 h after their addition (culture time 16 h), and the cellular uptake would be fairly rapid and can be

dx.doi.org/10.1021/ic500609g | Inorg. Chem. 2014, 53, 6817−6827

already observed at a time of 6 h (culture time 18 h) in Figure 8 (upper right). The fluorescence imaging occupation over the adhered cells was approximately several percent. With an increase in the culture time, the number of emitting nanospheres in the cells increased. At a time of 24 h after their addition (culture time 36 h), luminescence and cell aggregation shapes were clearly observed (Figure 8 (lower right)), and the fluorescent imaging occupation over the adhered cells was approximately 70−80%, which is 9−11 times higher than that over the adhered fibroblasts, indicating that the targeted nanosphere amounts are abundant for the Hela cells. Accordingly, it is suggested that FA-Eu:NPS was effectively taken up only by the Hela cells. Therefore, the obtained FA3-Eu:NPS can be readily taken up by the HeLa cells at the initial culture time and used as potential fluorescentce labels in biomedical imaging.

Figure 9 shows the luminescence intensity changes from the Hela cells that reacted with FA-Eu:NPS versus the culture time.

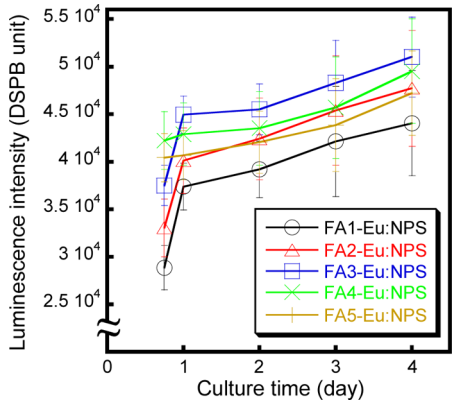

Figure 9. Luminescence intensity changes from the Hela cells reacted with FA-Eu:NPS versus culture time.

Here, the intensity was subtracted from that of the Hela cells alone. The apparent luminescence intensity from the Hela cells with the FA3-Eu:NPS nanospheres was saturated at a culture time of 24 h, and then that from the Hela cells gradually increases with the culture time. The intensities were almost the same irrespective of the FA functionalization amount, suggesting that the Hela cells realize the FA ligand and completely uptake FA-Eu:NPS during the initial 12 h. The uptake processes as well as the cell functions (e.g., proliferation) then effectively cause suppression of the luminescence quenching due to the nanosphere aggregation on/in the cell surfaces. Therefore, these results suggest that the Hela cells clearly realize the FA ligands and uptake FA-Eu:NPS during the initial stage.

Conclusions and Future Perspectives. FA was successfully functionalized on the luminescent Eu:NPS nanosphere surfaces by the mediation of the APTES adlayer. The ordered nanostructures were preserved by the functionalization. The FA-functionalized Eu:NPS nanospheres exhibited a new characteristic luminescence peak due to the interactions between FA and Eu^{3+}. The nanospheres, which were highly dispersed in cell culture medium, exhibited a high cytocompatibility against Hela cells and fibroblasts and were specifically bound to the Hela cells. The orange luminescence from the Hela cells was clearly detected by fluorescence microscopy. Therefore, the FA-functionalized nanospheres can be used as targeting against the cancer cells.

The linking of additional anticancer drug molecules into the nanopores is straightforward,[20] which could lead to further increases in the approach to various cancer-type therapies. As cancer cells typically overexpress multiple types of surface receptors, we are also focusing on ligands reacting with amino groups,[49] which are currently under study in our laboratories. Thus, the multicoupling of the functions in this study (e.g., targeting, imarging) as well as anticancer drugs in a sufficient concentration on one nanosphere can be achieved for both diagnosis and therapy.

■ ASSOCIATED CONTENT

Supporting Information

UV−visible absorption spectra of the DMSO solution containing NHS-FA at different concentrations, standard curve between the NHS-FA concentration and absorbance at 362 nm, scheme of the representative incident, scattering, and luminescence light intensity spectra for the calculation of internal quantum efficiency, transmitted bright-field images of the Hela cells and fibroblasts at a culture time of 60 h, transmitted bright-field and fluorescent images of Hela cells and fibroblasts without addition of nanosphres at a culture time of 24 h, incident, scattering, and luminescence light intensity spectra of Eu_2O_3 and Eu:NPS with different Eu concentrations, FT-IR spectra of Eu:NPS immobilized with APTES at different reaction times, TG and DTA curves of Eu:NPS immobilized with APTES at different reaction times, scheme of the FA incorporation into the external and internal nanopore surfaces, excitation and luminescence spectra of the neat FA and NHS-FA powder, photographs of bright-field and fluorescent images of FA3-Eu:NPS in PBS at a concentration of 500 μg/mL, and transmitted bright-field and fluorescent images of fibroblasts at different culture times after the addition of FA3-Eu:NPS. This material is available free of charge via the Internet at http://pubs.acs.org.

■ AUTHOR INFORMATION

Corresponding Author

*M.T.: tel, +81-258-47-9345; fax, +81-258-47-9300; e-mail, tagaya@mst.nagaokaut.ac.jp.

Notes

The authors declare no competing financial interest.

■ ACKNOWLEDGMENTS

This work was partially supported by a Grant-in-Aid for Challenging Exploratory Research (Grant No. 24651133) of MEXT/JSPS KAKENHI. This study was also partially supported by a Grant-in-Aid for the Adaptable and Seamless Technology Transfer Program through target-driven R&D (A-STEP: No. AS251Z00303P) of the Japan Science and Technology Agency (JST).

■ REFERENCES

(1) Brandon-Peppas, L.; Blanchette, J. O. *Adv. Drug Delivery* **2004**, *56*, 1649−1659.
(2) Caruso, F. *Adv. Mater.* **2001**, *13*, 11−22.
(3) Hu, L.; Mao, Z. W.; Gao, C. Y. *J. Mater. Chem.* **2009**, *19*, 3108−3115.
(4) Yanagisawa, T.; Shimizu, T.; Kuroda, K.; Kato, C. *Bull. Chem. Soc. Jpn.* **1990**, *63*, 988−992.
(5) Kresge, C. T.; Leonowicz, M. E.; Roth, W. J.; Vartuli, J. C.; Beck, J. S. *Nature* **1992**, *359*, 710−712.

(6) Beck, J. S.; Vartuli, J. C.; Roth, W. J.; Leonowicz, M. E.; Kresge, C. T.; Schmitt, K. D.; Chu, C. T. W.; Olson, D. H.; Sheppard, E. W.; McCullen, S. B.; Higgins, J. B.; Schlenker, J. L. *J. Am. Chem. Soc.* **1992**, *114*, 10834−10843.
(7) Yoon, K. B. *Chem. Rev.* **1993**, *93*, 321−339.
(8) M?ller, K.; Bein, T. *Chem. Mater.* **1998**, *10*, 2950−2963.
(9) Ogawa, M. *Annu. Rep. (Sect. C)* **1998**, *94*, 209−257.
(10) Stein, A.; Melde, B. J.; Schroden, R. C. *Adv. Mater.* **2000**, *12*, 1403−1419.
(11) Scott, B. J.; Wirnsberger, G.; Stucky, G. D. *Chem. Mater.* **2001**, *13*, 3140−3150.
(12) Furukawa, H.; Watanabe, T.; Kuroda, K. *Chem. Commun.* **2001**, 2002−2003.
(13) Ogawa, M. *J. Photochem. Photobiol. C: Photochem.* **2002**, *3*, 129−146.
(14) Mal, N. K.; Fujiwara, M.; Tanaka, Y. *Nature* **2003**, *421*, 350−353.
(15) Tagaya, M.; Ogawa, M. *Chem. Lett.* **2006**, *35*, 108−109.
(16) Tagaya, M.; Ogawa, M. *Phys. Chem. Chem. Phys.* **2008**, *10*, 6849−6855.
(17) Tagaya, M.; Hanagata, N.; Kobayashi, T. *ACS Appl. Mater. Interfaces* **2012**, *4*, 6169−6175.
(18) Vallet-Regi, M.; Balas, F.; Arcos, D. *Angew. Chem., Int. Ed.* **2007**, *46*, 7548−7558.
(19) Manzano, M.; Vallet-Regi, M. *J. Mater. Chem.* **2010**, *20*, 5593−5604.
(20) Tagaya, M.; Motozuka, S.; Kobayashi, T.; Ikoma, T.; Tanaka, J. *J. Mater. Chem.* **2012**, *22*, 18741−18743.
(21) Yang, P. P.; Gai, S. L.; Lin, J. *Chem. Soc. Rev.* **2012**, *41*, 3679−3698.
(22) Ruiz-Hitzky, E.; Aranda, P.; Darder, M.; Ogawa, M. *Chem. Soc. Rev.* **2011**, *40*, 801−828.
(23) Nassif, N.; Livage, J. *Chem. Soc. Rev.* **2011**, *40*, 849−859.
(24) Vivero-Escoto, J. L.; Slowing, I. I.; Wu, C. W.; Lin, V. S. Y. *J. Am. Chem. Soc.* **2009**, *131*, 3462−3463.
(25) Okuda, M.; Takeguchi, M.; Zhu, Y.; Hashimoto, A.; Ogawa, N.; Tagaya, M.; Chen, S.; Hanagata, N.; Ikoma, T. *Surf. Interface Anal.* **2010**, *42*, 1548−1551.
(26) Rosenholm, J. M.; Meinander, A.; Peuhu, E.; Niemi, R.; Eriksson, J. E.; Sahlgren, C.; Lindn, M. *ACS Nano* **2009**, *3*, 197−206.
(27) Sokolova, V.; Epple, M. *Nanoscale* **2011**, *3*, 1957−1962.
(28) Bardi, G.; Malvindi, M. A.; Gherardini, L.; Costa, M.; Pompa, P. P.; Cingolani, R.; Pizzorusso, T. *Biomaterials* **2010**, *31*, 6555−6566.
(29) Pan, J.; Wan, D.; Gong, J. L. *Chem. Commun.* **2011**, *47*, 3442−3444.
(30) Cheng, Z. Y.; Ma, P. A.; Hou, Z. Y.; Wang, W. X.; Dai, Y. L.; Zhai, X. F.; Lin, J. *Dalton Trans.* **2012**, *41*, 1481−1489.
(31) Kumar, R.; Roy, I.; Hulchanskyy, T. Y.; Goswami, L. N.; Bonoiu, A. C.; Bergey, E. J.; Tramposch, K. M.; Maitra, A.; Prasad, P. N. *ACS Nano* **2008**, *2*, 449−456.
(32) Zhu, Y.; Ikoma, T.; Hanagata, N.; Kaskel, S. *Small* **2010**, *6*, 471−478.
(33) Kang, X.; Huang, S.; Yang, P.; Ma, P.; Yanga, D.; Lin, J. *Dalton Trans.* **2011**, *40*, 1873−1879.
(34) Tagaya, M.; Ikoma, T.; Yoshioka, T.; Minami, F.; Tanaka, J. *Mater. Lett.* **2011**, *65*, 2287−2290.
(35) Tagaya, M.; Ikoma, T.; Yoshioka, T.; Tanaka, J. *J. Colloid Interface Sci.* **2011**, *363*, 456−464.
(36) Tagaya, M.; Ikoma, T.; Yoshioka, T.; Tanaka, J. *Chem. Commun.* **2011**, *47*, 8430−8432.
(37) Tagaya, M.; Hanagata, N.; Ikoma, T.; Kobayashi, T.; Shiba, K.; Yoshioka, T.; Tanaka, J. *Key Eng. Mater.* **2013**, *529*−*530*, 630−635.
(38) Kukowska-Latallo, J. F.; Candido, K. A.; Cao, Z. Y.; Nigavekar, S. S.; Majoros, I. J.; Thomas, T. P.; Balogh, L. P.; Khan, M. K.; Baker, J. R. *Cancer Res.* **2005**, *65*, 5317−5324.
(39) van Steenis, J. H.; van Maarseveen, E. M.; Verbaan, F. J.; Verrijk, R.; Crommelin, D. J. A.; Storm, G.; Hennink, W. E. I. *J. Controlled Release* **2003**, *87*, 167−176.
(40) Mosmann, T. *J. Immunol. Methods* **1983**, *65*, 55−63.
(41) Zhao, X. S.; Lu, G. Q.; Whittaker, A. K.; Millar, G. J.; Zhu, H. Y. *J. Phys. Chem. B* **1997**, *101*, 6525−6531.
(42) Zaitoun, M. A.; Kim, T.; Lin, C. T. *J. Phys. Chem. B* **1998**, *102*, 1122−1125.
(43) Chen, W.; Sammynaiken, R.; Huang, Y. *J. Appl. Phys.* **2000**, *88*, 1424−1431.
(44) Wan, N.; Xu, J.; Lin, T.; Zhang, X.; Xu, L. *Appl. Phys. Lett.* **2008**, *92*, 201109−201111.
(45) Nassar, E. J.; Ciuffi, K. J.; Ribeiro, S. J. L.; Messaddeq, Y. *Mater. Res.* **2003**, *6*, 557−562.
(46) Slowing, I. I.; Trewyn, B. G.; Lin, V.S.-Y. *J. Am. Chem. Soc.* **2006**, *128*, 14792−14793.
(47) Yu, K. O.; Grabinski, C. M.; Schrand, A. M.; Murdock, R. C.; Wang, W.; Gu, B.; Schlager, J. J.; Hussain, S. M. *J. Nanopart. Res.* **2009**, *11*, 15−24.
(48) Chan, S. Y.; Empig, C. J.; Welte, F. J.; Speck, R. F.; Schmaljohn, A.; Kreisberg, J. F.; Goldsmith, M. A. *Cell* **2001**, *106*, 117−126.
(49) Saul, J. M.; Annapragada, A. V.; Bellamkonda, R. V. *J. Controlled Release* **2006**, *114*, 277−287.